Title	The effects of high-pressure compression on transport and thermoelectric properties of TiS2 at low temperatures from 5 to 310K
Author(s)	Li, D.; Qin, X. Y.; Li, H. J.; Zhang, J.; Hng, Huey Hoon
Citation	Li, D., Qin, X. Y., Li, H. J., Zhang, J. & Hng, H. H. (2008). The effects of high-pressure compression on transport and thermoelectric properties of TiS2 at low temperatures from 5 to 310K. Journal of applied physics, 103(12), 123704-.
Date	2008
URL	http://hdl.handle.net/10220/18825
Rights	© 2008 American Institute of Physics. This paper was published in Journal of Applied Physics and is made available as an electronic reprint (preprint) with permission of American Institute of Physics. The paper can be found at the following official URL: [http://dx.doi.org/10.1063/1.2938748]. One print or electronic copy may be made for personal use only. Systematic or multiple reproduction, distribution to multiple locations via electronic or other means, duplication of any material in this paper for a fee or for commercial purposes, or modification of the content of the paper is prohibited and is subject to penalties under law.

The effects of high-pressure compression on transport and thermoelectric properties of TiS_2 at low temperatures from 5 to 310 K

D. Li,[1] X. Y. Qin,[1,a)] H. J. Li,[1] J. Zhang,[1] and Hng Huey Hoon[2]
[1]*Key Laboratory of Materials Physics, Institute of Solid State Physics, Chinese Academy of Sciences, 230031 Hefei, People's Republic of China*
[2]*School of Materials Science and Engineering, Nanyang Technological University, 639798, Singapore*

(Received 6 December 2007; accepted 5 April 2008; published online 17 June 2008)

The effects of high-pressure compression on the transport and thermoelectric properties of TiS_2 were investigated at temperatures ranging from 5 to 310 K. The results indicated that compression under the pressure of 6 GPa caused a significant decrease (16-fold at 300 K) in the absolute thermopower $|S|$ and the thermal conductivity (5-fold at 300 K). At the same time, the electrical resistivity ρ increased by two orders of magnitude after the compression. A transition from metallic state ($d\rho/dT>0$) to semiconductorlike state ($d\rho/dT<0$) was found to occur after the compression. This transition to the semiconductorlike state could be caused by the substantially enhanced grain boundary (GB) scattering due to the refinement of its grains to the nanoscale range, which should also be responsible for the remarkable increase in the resistivity and large decrease in thermal conductivity. Moreover, Mott's two-dimensional variable range hopping law, $\ln \rho \propto T^{-1/3}$, was observed at $T<\sim 100$ K for TiS_2 after the compression, suggesting that substantial potential disorder was produced by the high-pressure compression. The significant decrease of $|S|$ could originate from the possible compositional disorder in the GBs of TiS_2 after compression. The thermoelectric figure of merit of TiS_2 decreased after the compaction due to the large decrease in $|S|$ and increase in ρ, indicating that high-pressure compression is not beneficial to the thermoelectric performance of TiS_2. © *2008 American Institute of Physics*. [DOI: 10.1063/1.2938748]

I. INTRODUCTION

TiS_2 has an anisotropic structure with a trigonal space group $P\bar{3}m$. It is known to exist in two polytypes (1*T* and 2*H*) with octahedral and trigonal-prismatic coordinations, respectively. The main difference between the 1*T*-TiS_2 and 2*H*-TiS_2 layers is in the type of local coordination of metal: octahedral (1*T*) versus trigonal prismatic (2*H*).[1] The most stable form of TiS_2 (1*T*-TiS_2 crystallizes in a layered CdI_2-like structure) consists of sheets of face-sharing TiS_6 octahedra formed from S–Ti–S sandwich layers, where a Ti sheet is sandwiched between two sulfur sheets. Atoms within the S–Ti–S sheets are bound by strong covalent interactions, while bonding between the layers is determined by weak van der Waals forces.

Although the structure of TiS_2 is quite simple, the nature of the electronic structure of the layered material has been in dispute over the past decades, especially issues concerning whether it is a semimetal or a semiconductor.[2–13] For the semimetal model, there exists a small indirect overlap between the chalcogen-based valence *p* band at Γ (zone center) and the transition-metal-based conduction *d* band at *L* (zone boundary), while for the semiconductor model, there is an indirect energy gap between these two bands. Theoretical calculations have indicated that TiS_2 is a semimetal. Benesh *et al.*[2] showed that a semimetallic ground state exists in TiS_2 by using the linearized-augmented-plane-wave (LAPW) method. Other band calculations based on the augmented spherical wave method,[9] the linear-muffin-tin-orbital method,[3–5] and the full potential LAPW method[6,7] also showed similar results. However, experimental evidences such as the optical measurements of Greenway and Nitsche[8] indicated that TiS_2 is a semiconductor with a gap of 1–2 eV. Fang *et al.*[9] and Barry *et al.*[10] also reported a band gap of about 0.3 eV from angle-resolved photoemission studies. Photoemission experiments by Shepherd and Williams[11] indicated a band gap of less than 0.5 eV. In addition, many experiments[12,13] indicated that the electrical resistivity of TiS_2 almost exclusively exhibits a metallic behavior. Resistivity measurements in highly stoichiometric titanium disulfide indicate a metallic behavior at all temperatures.[14–16] However, up until now, no semiconductor behavior in the electrical resistivity of TiS_2 has ever been observed experimentally. Hence, it is of great importance for one to clarify the observed contradictory phenomena concerning the properties of TiS_2.

The use of pressure often causes the closing of band gap in low dimensional semiconductors.[17] This is usually associated with a structural phase transition.[18] It has been reported that the transport properties of TiS_2 (Ref. 19) showed pronounced discontinuities in the pressure dependence of both the Hall coefficient and the thermoelectric power at ≥ 4 GPa. The pressure dependence of the transport properties was found to be similar to those of semimetallic $TiSe_2$.

In this paper, we focused on the effects of high-pressure compression on the thermoelectric properties of TiS_2 prepared by gas-solid reaction. It was found that after compression under high pressure (6 GPa), significant changes in the transport and thermoelectric properties of TiS_2 occurred. The

a)Author to whom correspondence should be addressed. Electronic mail: xyqin@issp.ac.cn. FAX: 86-551-5591434. Tel.: 86-551-5592750

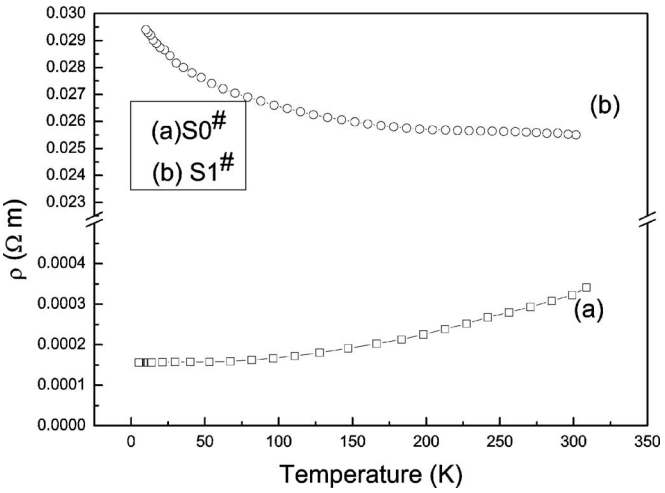

FIG. 1. Dependence of the electrical resistivity ρ on temperature for (a) S0# and (b) S1#.

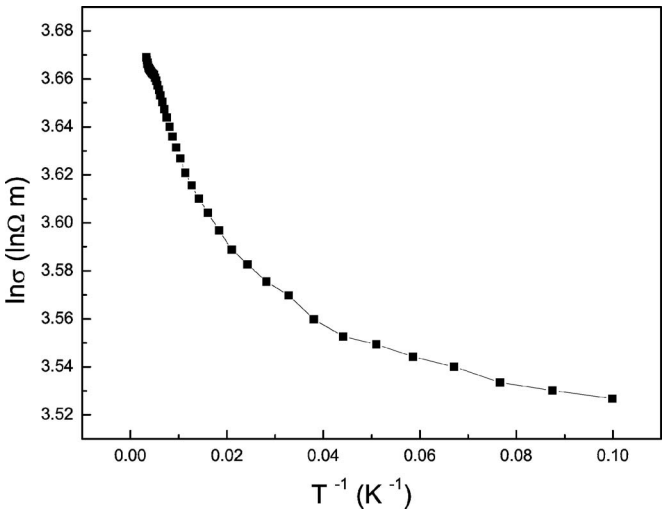

FIG. 2. Plot of ln σ vs $1/T$ for S1#.

changes were not associated with any structural phase transition in TiS_2. A possible underlying mechanism was discussed.

II. EXPERIMENTAL METHODS

TiS_2 powder was prepared by direct reactions (in an evacuated quartz ampoule) of titanium metal powder (99.7%) and sulfur powder (99.5%) at 610 °C for 7 days. The powders were pressed into pellets under 250 MPa and wrapped with silver foil at room temperature. It was then compressed (via a medium composed of NaCl and pyrophyllite) at room temperature under a pressure of 6 GPa for 30 min by using a cubic anvil. Bar-shaped specimens with size of $6\times3\times(\sim)1.5$ mm^3 (sample S1#) were cut from the compressed bulk samples for measurements. For comparison, TiS_2 powders were compacted by hot pressing (under the pressure of 300 MPa) in vacuum at 400 °C to obtain bulk samples with size of $30\times10\times(\sim)1.5$ mm^3. Bar-shaped specimens with size of $13\times2\times(\sim)1.5$ mm^3 (sample S0#) were cut from the hot-pressed samples for measurements.

The phase structure of TiS_2 before and after high-pressure compaction was analyzed by using x-ray diffraction (XRD) (X'Pert Pro MPD). Microstructures of the TiS_2 samples were observed using field-emission scanning electron microscopy (FESEM) (Sirion 200). Four probes (Cu straps) were electrically and thermally attached to the specimens with silver conductive adhesive paste (Phentex Corp. USA) to measure their electrical resistances. When thermopower and thermal conductivity were measured, the middle two probes were used to determine temperature gradient (difference) and potential difference. The thermoelectric properties (electrical resistance, thermopower, and thermal conductivity) were measured simultaneously by using a physical property measurement system (Quantum Design, USA) in the temperature range of 5–310 K.

III. RESULTS

Figure 1 shows the variations of electrical resistivity ρ with temperature for sample S0# [curve (a)] and sample S1# [curve (b)]. By comparing these two curves, it is noted that there is a significant increase in the resistivity of TiS_2 after high-pressure compression. For example, at 300 K, ρ increases from 3.20×10^{-4} Ω m for S0# to 2.55×10^{-2} Ωm for S1#, and at 5 K it increases from 1.58×10^{-4} Ω m for S0# to 2.93×10^{-2} Ω m for S1#. In addition, the temperature dependence of resistivity is also affected by the high-pressure compression. The ρ-T curve for sample S0# shows a metal-like behavior (i.e., $d\rho/dT>0$) for the whole temperature range investigated [curve (a)]. Fitting the resistivity to a power law, $(\rho(T)-\rho_0)\propto T^{\gamma}$, gives $\gamma=2.2$. This value is in agreement with previous results reported by Klipstein *et al.*[20] On the other hand, the ρ-T curve for sample S1# displays semiconductorlike behavior ($d\rho/dT<0$) in the whole temperature range investigated. By plotting ln σ vs $1/T$ (Fig. 2) for sample S1#, it is noted that a linear relationship is not obtained. This suggests that the electrical conduction in sample S1# is not dominated by a simple thermal activation process over the entire temperature range investigated here.

Figure 3 gives the thermopower as a function of temperature for S0# and S1#. The thermopower for both samples are negative, indicating that electrons are the major charge

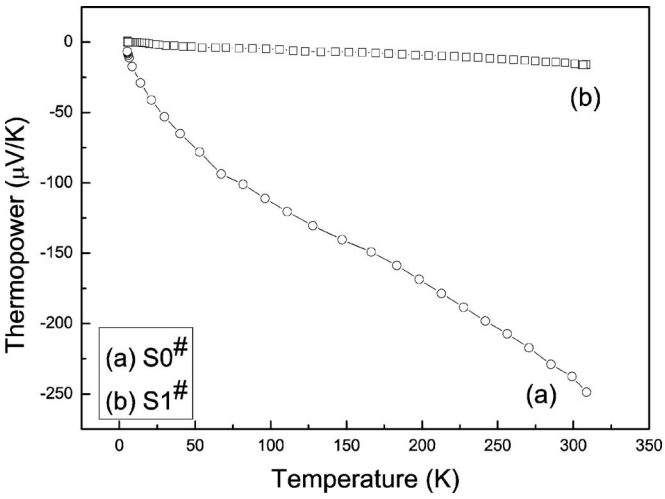

FIG. 3. Variation of thermopower with temperature for (a) S0# and (b) S1#.

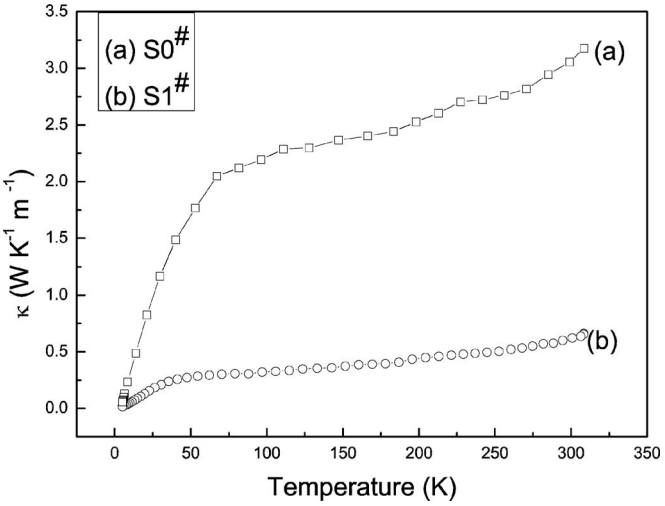

FIG. 4. Plot of thermal conductivity κ vs temperature for (a) S0# and (b) S1#.

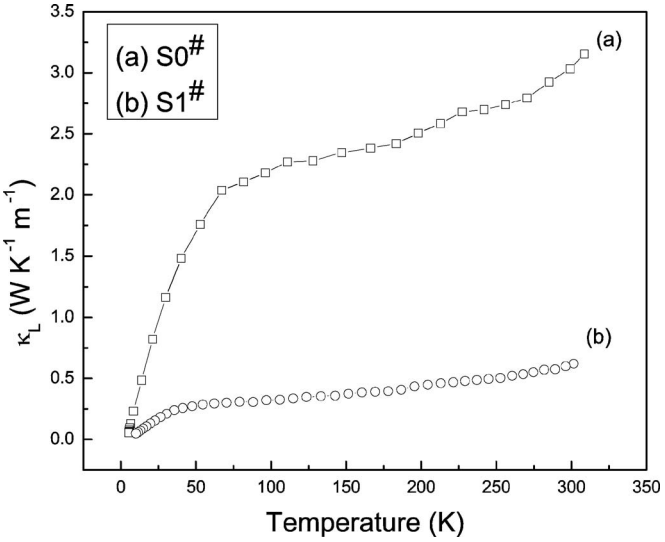

FIG. 5. Plot of lattice thermal conductivity κ_L vs temperature for (a) S0# and (b) S1#.

carriers in TiS_2 before and after high-pressure compression over the entire temperature range. However, it can be seen clearly that after compression under high pressure, the absolute thermopower $|S|$ of TiS_2 decreases abruptly [curve (b) in Fig. 3]. For example, thermopowers at 300 K are −240 and −15 μV/K for S0# and S1#, respectively. Furthermore, the absolute value of the slope of the *S*-*T* curve for S1# becomes much smaller than that for S0#. The small valley around 50 K observed in curve (a) for sample S0#, which is presumably caused by the phonon-drag effect,[21] hardly appeared in curve (b) for sample S1#. The current results indicate that the thermopower of TiS_2 is strongly affected by the high-pressure compression.

Temperature dependences of thermal conductivity κ for TiS_2 before and after compaction are shown in Fig. 4. It can be seen that although the temperature dependence of κ for S1# is similar to that for S0#, κ for sample S1# is significantly lower than that for sample *S*0#. For example, at 300 K, κ decreases from 3.06 W m^{-1} K^{-1} for S0# to 0.63 W m^{-1} K^{-1} for S1#. Thermal conductivity κ can be expressed as the sum of the lattice component (κ_L) and the carrier component (κ_c): $\kappa=\kappa_L+\kappa_c$. The κ_c values can be estimated from Wiedemann–Franz's law as $\kappa_c=LT/\rho$, where L is the Lorentz number. As a semiquantitative estimation, we use the value L_0 of free electrons for L (i.e., $L=L_0=2.44\times10^{-8}$ V^2 K^{-2}) for both samples. Consequently, κ_L can be obtained from κ and κ_c, as shown in Fig. 5. By comparing Fig. 5 with Fig. 4, it can be seen that the total thermal conductivity of TiS_2 (both before and after compression) arises mainly from the lattice component. Likewise to the total thermal conductivity, the lattice component κ_L of S1# is much smaller than that of S0#. Specifically, κ_L of S1# at 300 K (0.60 W K^{-1} m^{-1}) is five times smaller than that of S0# (3.05 W K^{-1} m^{-1}).

The thermoelectric figure of merit, ZT ($=S^2T/(k\rho)$), is calculated for samples S1# and S0#, as shown in Fig. 6. The ZT for both the samples increases with increasing temperature. However, the ZT of S1# is a lot smaller than that of S0# due to the large decrease in thermopower and large increase in the resistivity of S1#, even though there was a considerable reduction in the thermal conductivity. This result shows that high-pressure compression is not beneficial to the thermoelectric performance of TiS_2.

IV. DISCUSSION

The above results indicate that the resisitivity, thermopower, and thermal conductivity of TiS_2 are strongly influenced by compression under a pressure of 6 GPa. The changes in transport and thermoelectric properties could be related to the evolution of its phase structure and/or microstructures during the high-pressure compression. In order to explore the underlying mechanisms, possible phase structure and microstructure changes were investigated. Figure 7 shows the XRD patterns obtained for samples S0# [curve (a)] and S1# [curve (b)]. All the main diffraction peaks in curve (b) match with those in curve (a), and they correspond to the crystallographic structure of 1*T*-TiS_2. Nevertheless, through careful inspection one could find that there is an additional

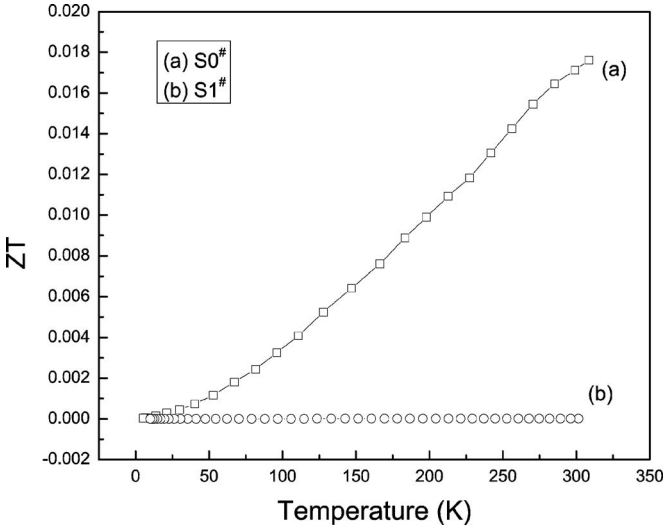

FIG. 6. Variation of ZT with temperature for (a) S0# and (b) S1#.

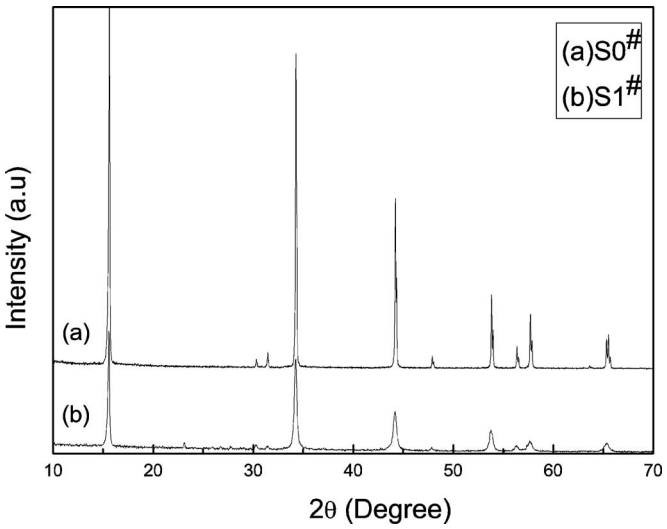

FIG. 7. The XRD patterns for (a) $S0^{\#}$ and (b) $S1^{\#}$.

small peak appearing at $2\theta \approx 23.1°$ on curve (b), which can be attributed to the residual of pyrophyllite (corresponding to the compound $Al_2O_{111}Si_{54}$ (JCPDS Card No. 044-0002), a main component of medium pyrophyllite) utilized in the compression process. This result indicates that the phase structure of TiS_2 was not changed due to the high-pressure compression. Moreover, one important difference in diffraction peaks for the two samples is that diffraction peaks of sample $S1^{\#}$ are broadened substantially, as compared to those of sample $S0^{\#}$. Such broadening of the diffraction peaks arises either from grain refinement or from lattice strain (i.e., lattice distortion) or from the consideration of both effects. The average grain size d of $S1^{\#}$ was estimated to be ~45 nm by using the Scherrer formula. This value is much smaller than that of the uncompressed sample $S0^{\#}$, which is in the micron range. To confirm the XRD results, the grain morphologies of both $S1^{\#}$ and $S0^{\#}$ were observed directly using FESEM, as shown in Fig. 8. It can be seen that most of the particles or grains of $S0^{\#}$ have the sizes of several micrometers to dozens of micrometers, while most of the grains of $S1^{\#}$ have sizes ranging from 30 to 60 nm (in agreement with the XRD results). The mean grain size of $S1^{\#}$ is several orders in magnitude smaller than that of $S0^{\#}$. The origin of this microstructural evolution into nanocrystalline structure may be due to the layered structure and very brittle nature of TiS_2. During compression under high pressure, TiS_2 has experienced severe deformation and would fracture into very fine pieces through shearing cracking along van der Waals layers in-between S–Ti–S slabs or/and bending failure across these slabs, or through complex combination of these failure modes.

The above result means that the contribution of grain boundaries (GBs) to the transport and thermoelectric properties in sample $S0^{\#}$ can be neglected, as has been done in other conventional polycrystalline materials. However, the contribution of GBs to the transport and thermoelectric properties in $S1^{\#}$ is expected to be too substantial to be neglected, as there is a large volume fraction of GBs (for a specimen with an average grain size of 45 nm, the volume fraction of GBs is ~6.7% in $S1^{\#}$ if the thickness of the GB is assumed

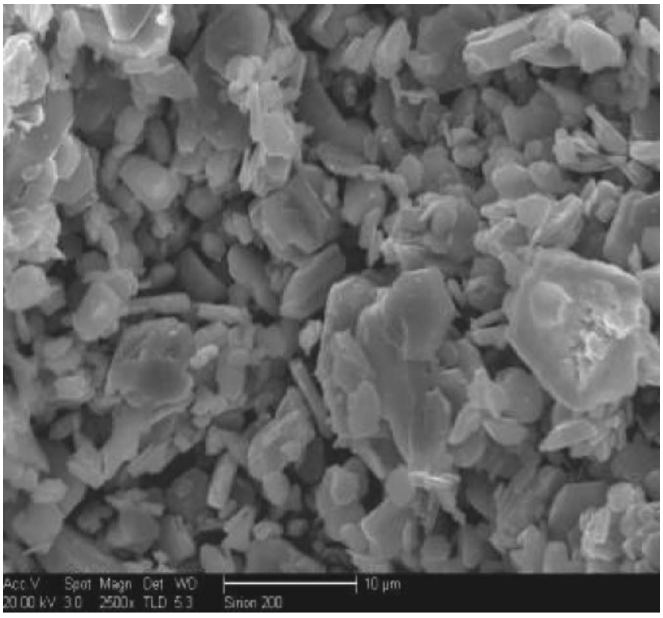

(a)

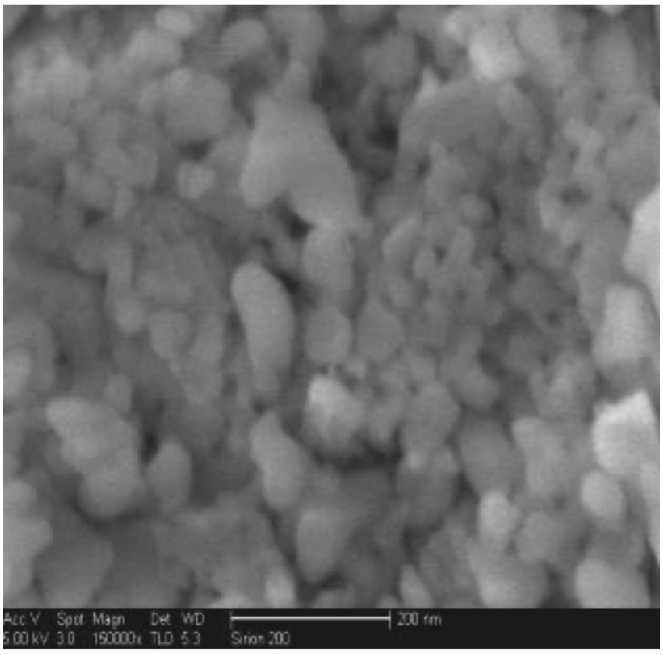

(b)

FIG. 8. FESEM observations on the grain morphologies of TiS_2: (a) $S0^{\#}$ and (b) $S1^{\#}$.

to be 1 nm[22]). As the compression was done at ambient temperature, the atoms and defects were randomly arranged in GBs since atomic relaxation is limited during and after compression, which will result in strong potential disorder. Hence, these GBs and the defects therein will form barriers and enhance the scattering of the carriers. However, as temperature increases, their ability to scatter carriers is expected to diminish due to enhanced thermal activation, and this will be manifested as the occurrence of semiconductorlike behavior (as seen in Fig. 1). When temperature is low enough, phonon-assisted variable range hopping (VRH) may dominate the conduction process. By fitting the experimental data to Mott's VRH law,

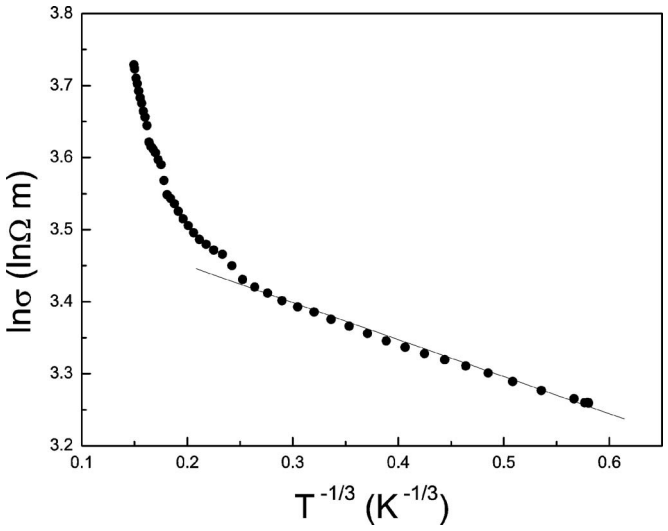

FIG. 9. Plot of ln σ vs $1/T^{1/3}$ for $S1^{\#}$. The solid line is the best fit of the data to formula (1) at $T<100$ K.

$$\sigma = \sigma_0 \exp\left[-\left(\frac{T_0}{T}\right)^{1/3}\right] \tag{1}$$

with

$$T_0 = 8/(\pi k N(E_F) L_v^2)$$

where T_0 is the hopping barrier, σ_0 is a constant, and k, $N(E_F)$, and L_v are the Boltzmann constant, the density of states at the Fermi level, and the localization length, respectively, it was found that the conductivity data for $S1^{\#}$ in the very low-temperature range ($T<\sim 100$ K) are in good agreement with Mott's two-dimensional (2D) VRH model (Fig. 9). This suggests that TiS_2 exhibited 2D transport characteristics and after high-pressure compression, substantial potential disorder could be produced. These potential disorders in GBs could also be responsible for the large increase in resistivity and remarkable decrease in lattice thermal conductivity of $S1^{\#}$.

As discussed above, random atomic arrangements, or structural disorders, in the GBs may give rise to potential disorder. In addition, considerable compositional disorders, such as dangling bonds and "wrong" bonds (Ti–Ti bonds or/and S–S bonds), may also exist concurrently in the incompletely relaxed GBs of nanograined TiS_2 with high ionicity. This can produce additional defect levels.[23] Although there would be no large difference in the producing probability of Ti–Ti wrong bonds and S–S wrong bonds in GBs, the quantity of respective dangling bonds may be different. Since bonding between the S–Ti–S slabs rely mainly on weak van der Waals forces, the probability of peeling off or fracture along the van der Waals layers in-between S–Ti–S slabs is expected to be much higher than that within S–Ti–S sheets or in other directions. In other words, dangling bonds of S atoms, which introduce acceptor states, would be overwhelmingly more than Ti dangling bonds. As a result, the GB regimes would become p type when the number of the defect is large enough. In other words, both n-type conduction (in intragranular regimes) and p-type conduction (in GB regimes) could coexist in $S1^{\#}$. This will inevitably lead to substantial decrease in the total thermopower for the sample since the positive thermopower coming from holes will counteract the (negative) thermopower coming from electrons.

V. CONCLUSIONS

The effects of high-pressure compression on the transport and thermoelectric properties of TiS_2 were investigated. The results indicated that high-pressure compression at 6 GPa not only caused a significant decrease in the absolute thermopower $|S|$ (16-fold at 300 K) but also a large drop (fivefold at 300 K) in the thermal conductivity. Moreover, the electrical resistivity was increased by two orders of magnitude after the compression. A transition from metallic state ($d\rho/dT>0$) to semiconductorlike state ($d\rho/dT<0$) was found to occur after the compression. This transition to semiconductorlike state could be caused by the substantially enhanced GB scattering due to the refinement of its microstructures. This could also explain the remarkable increase in the resistivity and decrease in the thermal conductivity. The experimental data showed that Mott's 2D VRH law occurred at $T<\sim 100$ K for TiS_2 after the compression. This suggests that a large potential disorder was produced due to the compression process. The large decrease in $|S|$ could be related to the possible compositional disorder in the GBs of TiS_2 after the compression. The thermoelectric figure of merit of TiS_2 decreased substantially after the compaction mainly due to a large decrease in $|S|$ and an increase in ρ, indicating that high-pressure compression is harmful to the thermoelectric performance of TiS_2.

ACKNOWLEDGMENTS

Financial support from the National Natural Science Foundation of China (Grant Nos. 50472097 and 10504034) is gratefully acknowledged.

[1] V. V. Ivanovskaya and G. Seifert, Solid State Commun. **130**, 175 (2004).
[2] G. A. Benesh, A. M. Woolley, and C. Umrigar, J. Phys. C **18**, 1595 (1985).
[3] Z. Y. Wu, G. Ouvrard, S. Lemaux, P. Moreau, P. Gressier, and F. Lemoigno, Phys. Rev. Lett. **77**, 2101 (1996).
[4] Z. Y. Wu, F. Lemoigno, P. Gressier, G. Ouvrard, P. Moreau, J. Rouxel, and C. R. Natoli, Phys. Rev. B **54**, R11009 (1996).
[5] Z. Y. Wu, G. Ouvrard, P. Moreau, and C. R. Natoli, Phys. Rev. B **55**, 9508 (1997).
[6] S. Sharma, T. Nautiyal, G. S. Singh, S. Auluck, P. Blaha, and C. Ambrosch-Draxl, Phys. Rev. B **59**, 14833 (1999).
[7] A. H. Reshak and S. Auluck, Phys. Rev. B **68**, 245113 (2003).
[8] D. L. Greenaway and R. T. Nitsche, J. Phys. Chem. Solids **26**, 1445 (1965).
[9] C. M. Fang, R. A. de Groot, and C. Haas, Phys. Rev. B **56**, 4455 (1997).
[10] J. J. Barry, H. P. Hughes, P. C. Klipstein, and R. H. Friend, J. Phys. C **16**, 393 (1983).
[11] F. R. Shepherd and P. M. Williams, J. Phys. C **7**, 4416 (1974).
[12] E. E. Abbott, J. W. Kolis, N. D. Lowhorn, W. Sams, and T. M. Tritt, *Thermoelectric Properties of TiS$_2$ Type Materials*, MRS Symposia Proceedings No. 793 (Materials Research Society, Pittsburgh, 2004), p. 295.
[13] C. A. Kukkonen, W. J. Kaiser, E. M. Logothetis, B. J. Blumenstock, P. A. Schroeder, S. P. Faile, R. Colella, and J. Gambold, Phys. Rev. B **24**, 1691 (1981).
[14] D. Li, X. Y. Qin, J. Liu, and H. S. Yang, Phys. Lett. A **328**, 493 (2004).
[15] A. Kukkonen, W. J. Kaiser, E. M. Logothetis, B. J. Blumenstock, P. A.

Schroeder, S. P. Faile, R. Colella, and J. Gambold, Phys. Rev. B **24**, 1691 (1981).
[16]H. Imai, Y. Shimaka, and Y. Kubo, Phys. Rev. B **64**, 241104 (2001).
[17]H. C. Hsueh, H. Vass, S. J. Clark, G. J. Ackland, and J. Crain, Phys. Rev. B **51**, 16750 (1995).
[18]H. Akbarzadeh, S. J. Clark, and G. J. Ackland, J. Phys.: Condens. Matter **5**, 8065 (1993).
[19]P. C. Klipstein and R. H. Friend, J. Phys. C **17**, 2713 (1984).
[20]P. C. Klipstein, A. G. Bagnall, W. Y. Liang, E. Z. Marseglia, and R. H. Friend, J. Phys. C **14**, 4067 (1981).
[21]D. Li, X. Y. Qin, J. Liu, and H. S. Yang, Phys. Lett. A **328**, 493 (2004).
[22]T. Mutschele and R. Kirchheim, Scr. Metall. **21**, 1101 (1987).
[23]E. P. O'Reilly and J. Robertson, Phys. Rev. B **34**, 8684 (1986).